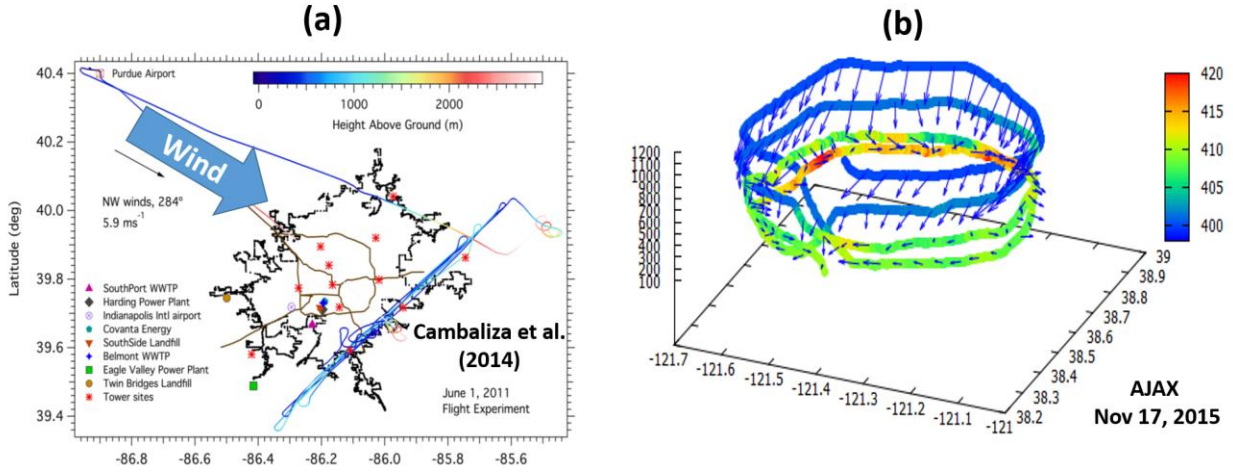

Figure S1: Comparison of flight design: (left) conventional curtain flight and (right) the cylindrical flight track. The arrows overlaid over the cylinder represent the 3-D wind measured in-situ.

Figure S1a shows the typical mass balance "curtain flight," which detects point sources and assumes that emissions are accumulated downwind. This typical flight pattern requires the prior knowledge of wind direction because this can be a critical factor in deciding where to measure. This flight pattern also ignores the vertical mass transfer from the top of the Planetary Boundary Layer (PBL) and from the surface. In contrast, Fig. S1b shows the same mass balance approach in conjunction with cylindrical flight pattern. Downwind regions do not always have the highest CO_2 values, which vary with location and altitude. Using this method, we can detect emissions from more than one point source within a city, both downwind and throughout the city. Also, while useful for planning, prior knowledge of wind direction is not necessary for measurements. Lastly, vertical mass transfer across the top and bottom of the cylinder can be estimated using this approach.

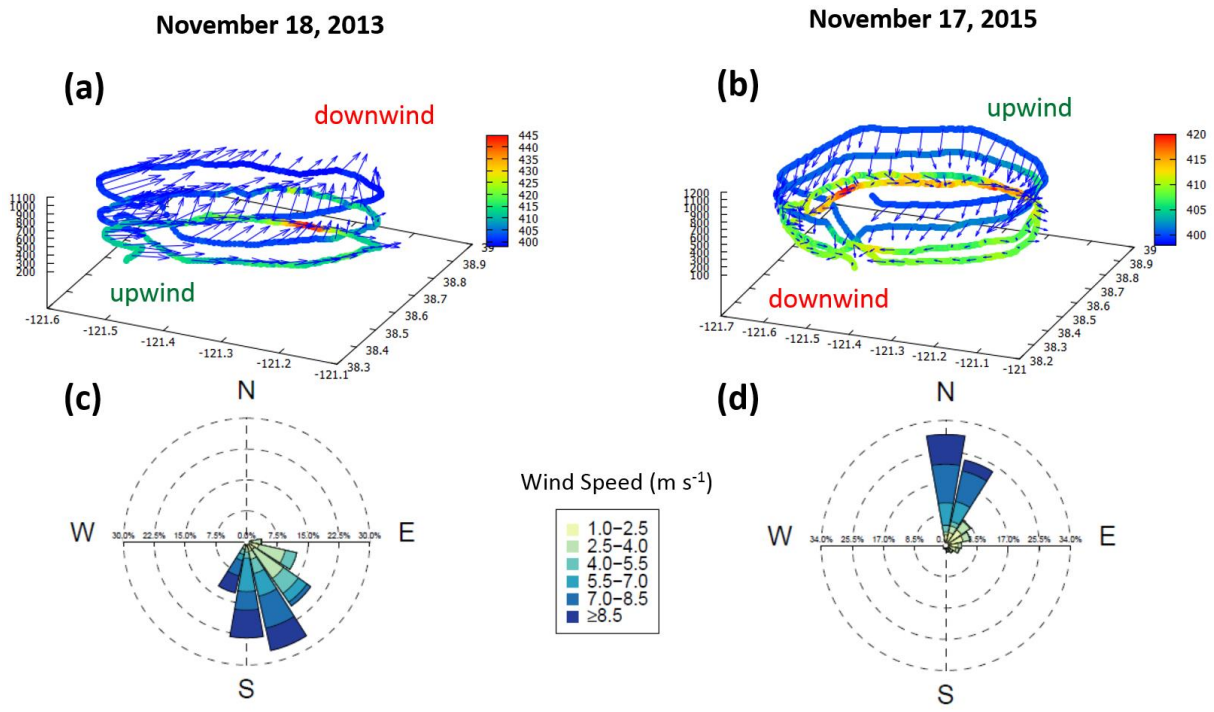

Figure S2: (a, b) Wind vectors overlaid on the flight track colored by observed CO_2 mixing ratio (c, d) Wind-rose map of the observed horizontal wind throughout the altitude over Sacramento on (left) November 18, 2013 and (right) November 17, 2015.

To see the effect of wind conditions on the measurements, we looked at the wind direction and its change with altitude on November 18, 2013, and November 17, 2015, as seen in Fig. S2. The wind directions on the two flight days were different. On November 18, 2013, the wind was primarily southerly or southeasterly; over the downwind northwestern segment, the CO_2 mixing ratio tended to be elevated in the lower altitude. On November 17, 2015, the downwind segment was mostly on the southern side of Sacramento, and high CO_2 was not seen to be accumulated over downwind due to low wind speed, especially in the lower altitudes (see Figs. S2(b, d)). The elevation of CO_2 in the lower altitude on the upwind side appeared to be attributed to a local source. The wind was very weak in the lower level on November 17, 2015, making the air more stable and less dispersive. Both flights illustrate that the wind can vary by altitude and location, even if measured on the same day within the same hour, or within a few kilometers. Therefore, relying on an assumption of "constant" regional or continental scale wind throughout the entire range of altitudes can produce biased flux estimates.

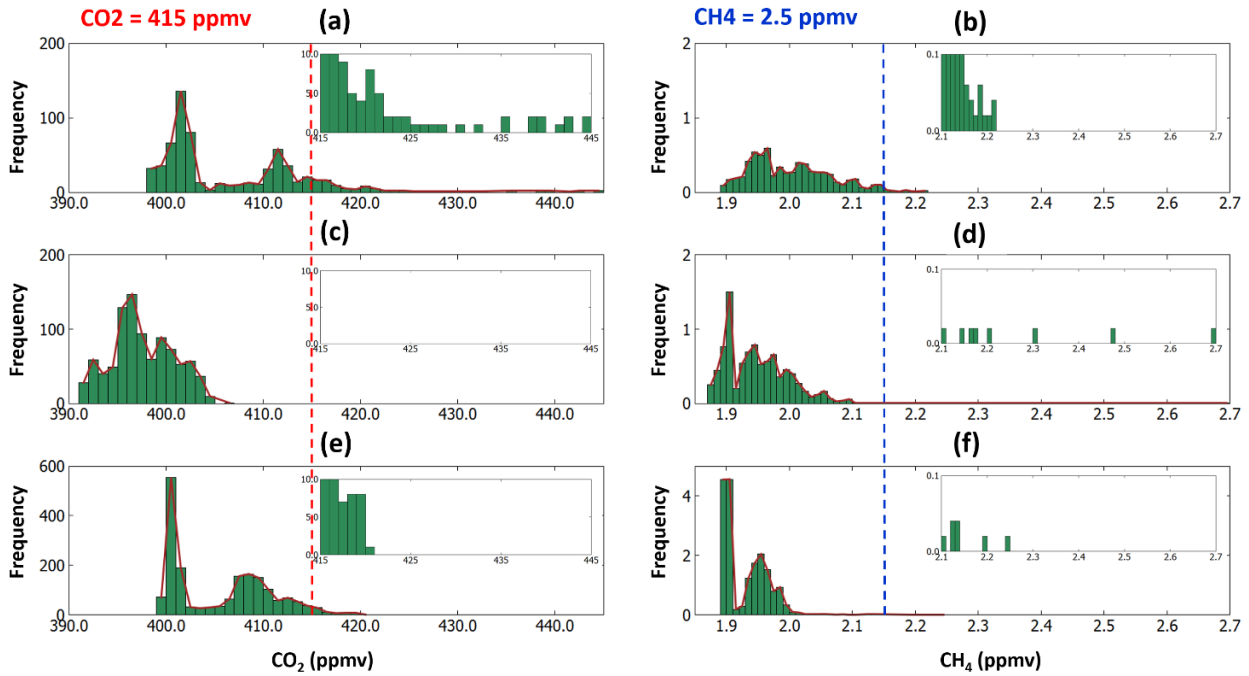

Figure S3: The probability distribution functions (pdf) of (left) CO_2 and (right) CH_4 mixing ratio over Sacramento on (a, b) November 18, 2013, (c, d) July 29, 2015, and (e, f) November 17, 2015. The insets expand the vertical axis for data falling to the right of the red dashed line (CO_2 = 415 ppm, CH_4 = 2.15 ppm) observation. In this histogram, CO_2 and CH_4 mixing ratios measured over the entire urban area of Sacramento are used.

Figure S3 displays the probability distribution functions (histograms) of (left) CO_2 and (right) CH_4. Both CO_2 and CH_4 for the two winter flights (November) show bimodal patterns, highlighting the difference between upwind and downwind sides of the city. But on the July 29 flight, there is also "intermediate" region of average high CH_4 mixing ratio. The largest peak for CH_4 was found (up to 2.7 ppmv) on July 29, 2015. CO_2 mixing ratio was greater in winter (November) than that in summer (July), but not a significant difference was found for CH_4. The high CO_2 values (> 415 ppmv) were only observed in winter, but the high CH_4 values (>2.15 ppmv) were found during both summer and winter. Although caution is required while ascribing "seasonality" to the CO_2 data from just two months, the seasonality implied is consistent with the previous studies and with the general characteristics of the CO_2 seasonal cycle (Dettinger and Ghil, 1998; Pataki et al., 2003).

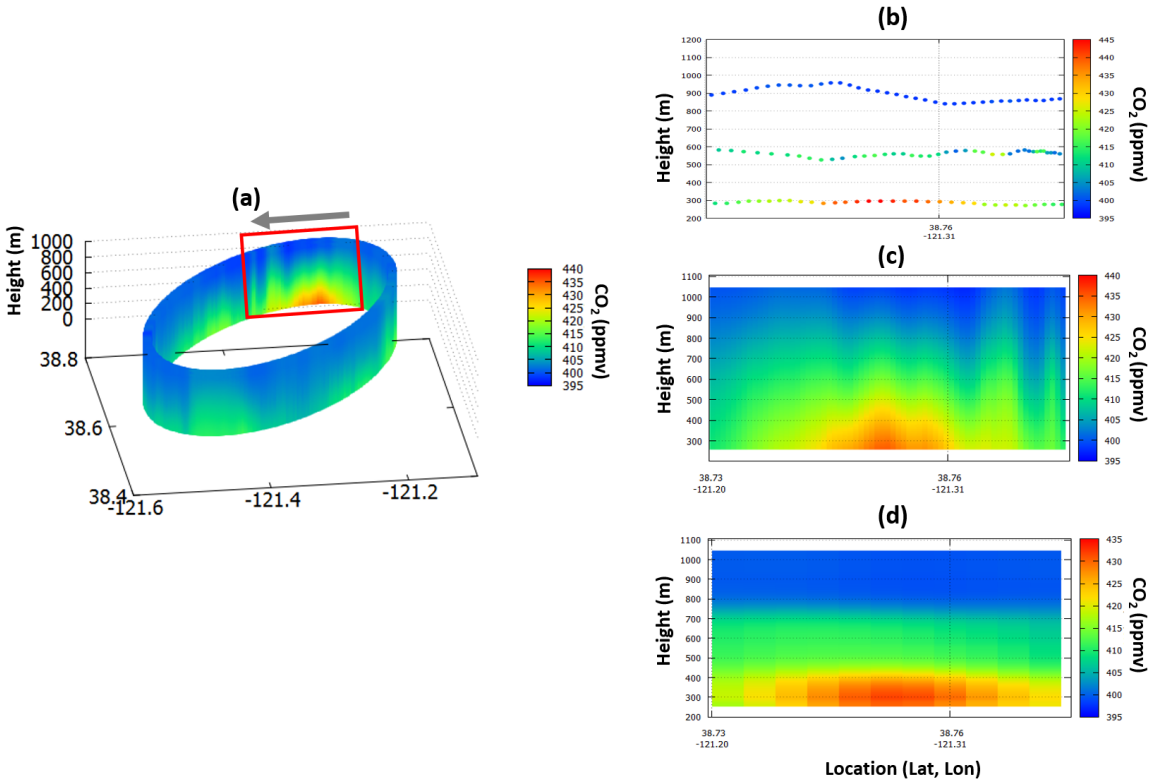

Figure S4: (a) Kriged CO_2 mixing ratio, (b) Measured CO_2 mixing ratio, (c) CO_2 mixing ratio using kriging interpolation method, (d) interpolated CO_2 mixing ratio using a conventional exponential weighting function along a subset of the ellipse around Sacramento on November 18, 2013. This portion of the perimeter corresponds to the red box of the elliptical cylinder shown in Figure S4a. The direction of the arrow represent the direction from left to right in figure S4c.

Figure S4 shows the observed CO_2 mixing ratio obtained by AJAX for a portion of the ellipse sampled in 2013, and the interpolated CO_2 mixing ratio calculated using ordinary kriging or an exponential weighting function. The interpolated value using the exponential weighting function is defined as the value at each point (P) as the weighted average of all the other points, where the weight of each decreases exponentially with its distance to P. As stated in the manuscript, both interpolation methods captured the general plume pattern (high and low concentration of CO_2 regions), but kriging interpolation did a better job in capturing the individual plume characteristics such as range and magnitude.

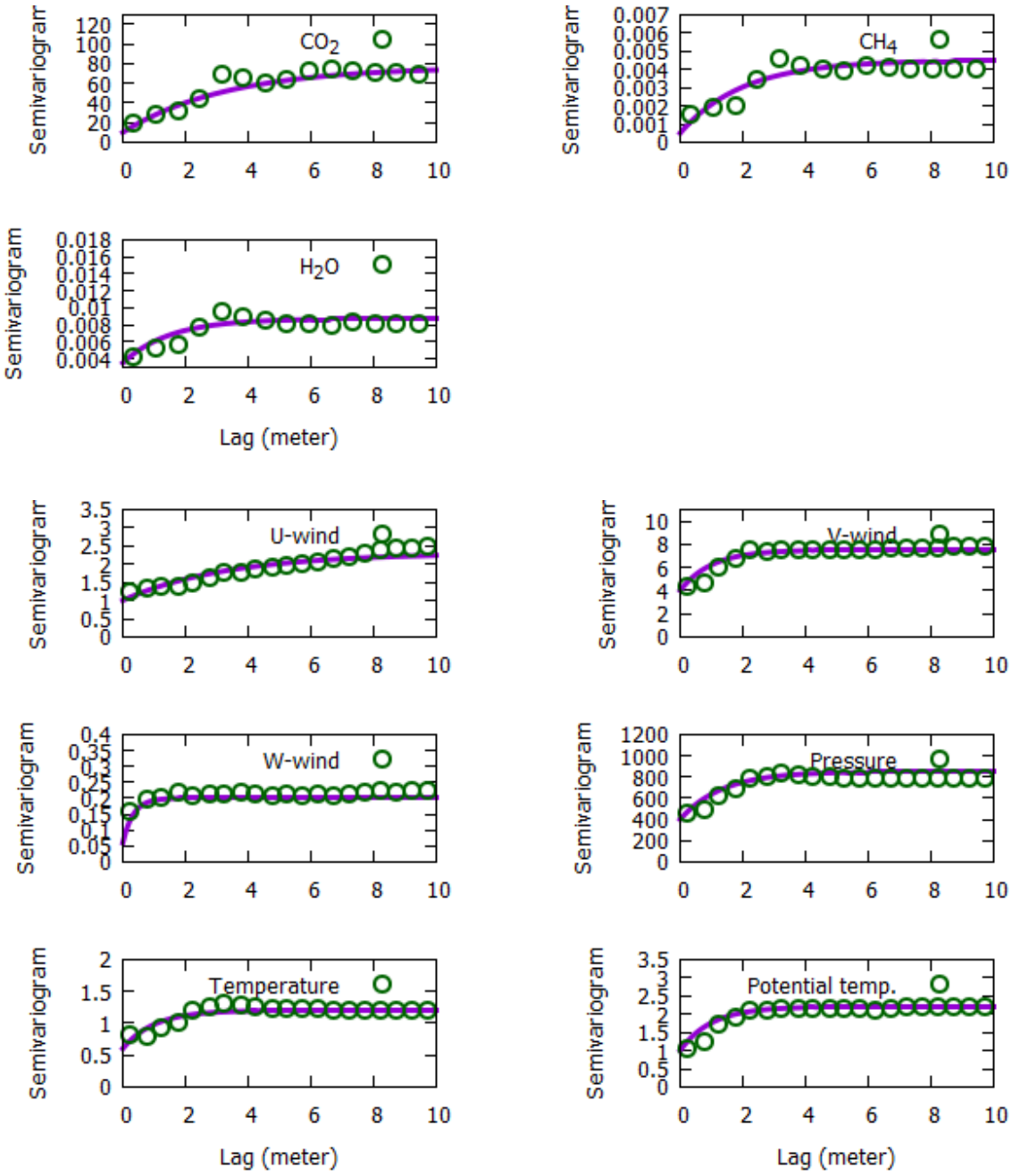

Figure S5: The experimental (open circle) and theoretical exponential (solid purple line) semivariograms of CO_2, CH_4, H_2O, 3-D winds (U, V, W), pressure, temperature, and potential temperature for the flight on November 18, 2013.

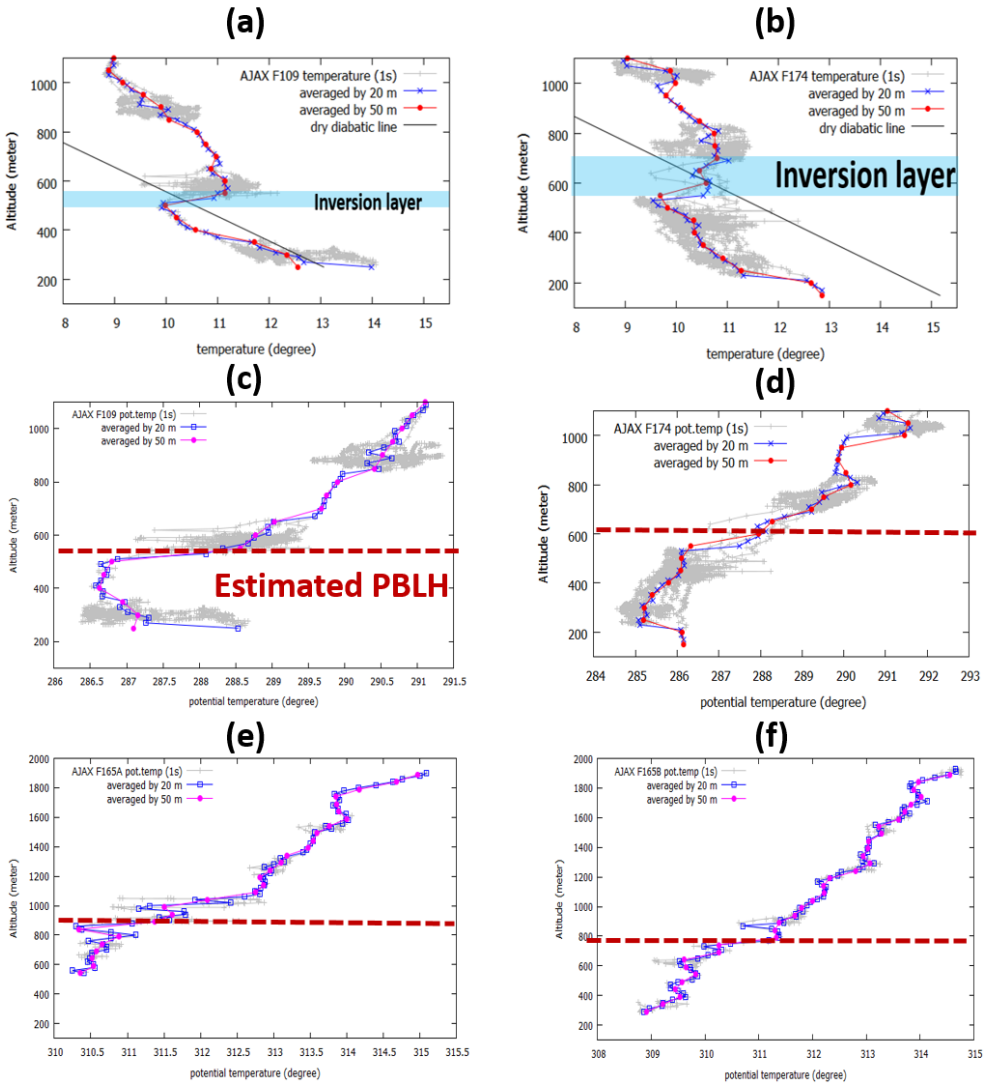

Figure S6: Meteorological data collected on three days: (a, c) November 2013, (b, d) November 2015, and (e, f) July 29, 2015.The top two panels shows temperature, and the remaining panels show potential temperature. Panel (e) is data collected in a spiral over a landfill, and the data in panel (f) were collected over a rice field. The dashed line indicates the estimated planetary boundary layer height (PBLH), identified by the maximum gradient of the potential temperature.

Local scale (< 3 km) - Small loops on July 29, 2015

To find the contribution from two local sources of particular importance, small loops (~ Z km in diameter) were flown over a landfill and a rice field shown in Fig. S7. The measured CO_2 and CH_4 are in Fig. S8. The enhancements of CO_2 and CH_4 were not collocated, indicating different point sources. For both CO_2 and CH_4, larger mixing ratios were detected over the landfill. The CH_4 enhancement was localized near the landfill. It has been known that landfills are large contributors to CH_4 emissions (Mays et al. 2009), and we confirm that detecting the large local source of CH_4 is necessary for estimating the CH_4 concentration and fluxes for Sacramento case. Due to the photosynthetic activity of plants during summer, CO_2 over the rice field appears to be low. The wind direction was mostly easterly or southeasterly over the landfill and mostly southerly over the rice field. The wind speed was

weaker over the landfill (mostly 1.0–2.5 m s^{-1}) than that over the rice field, indicating that the most of the methane observed over the landfill originated from that source.

90

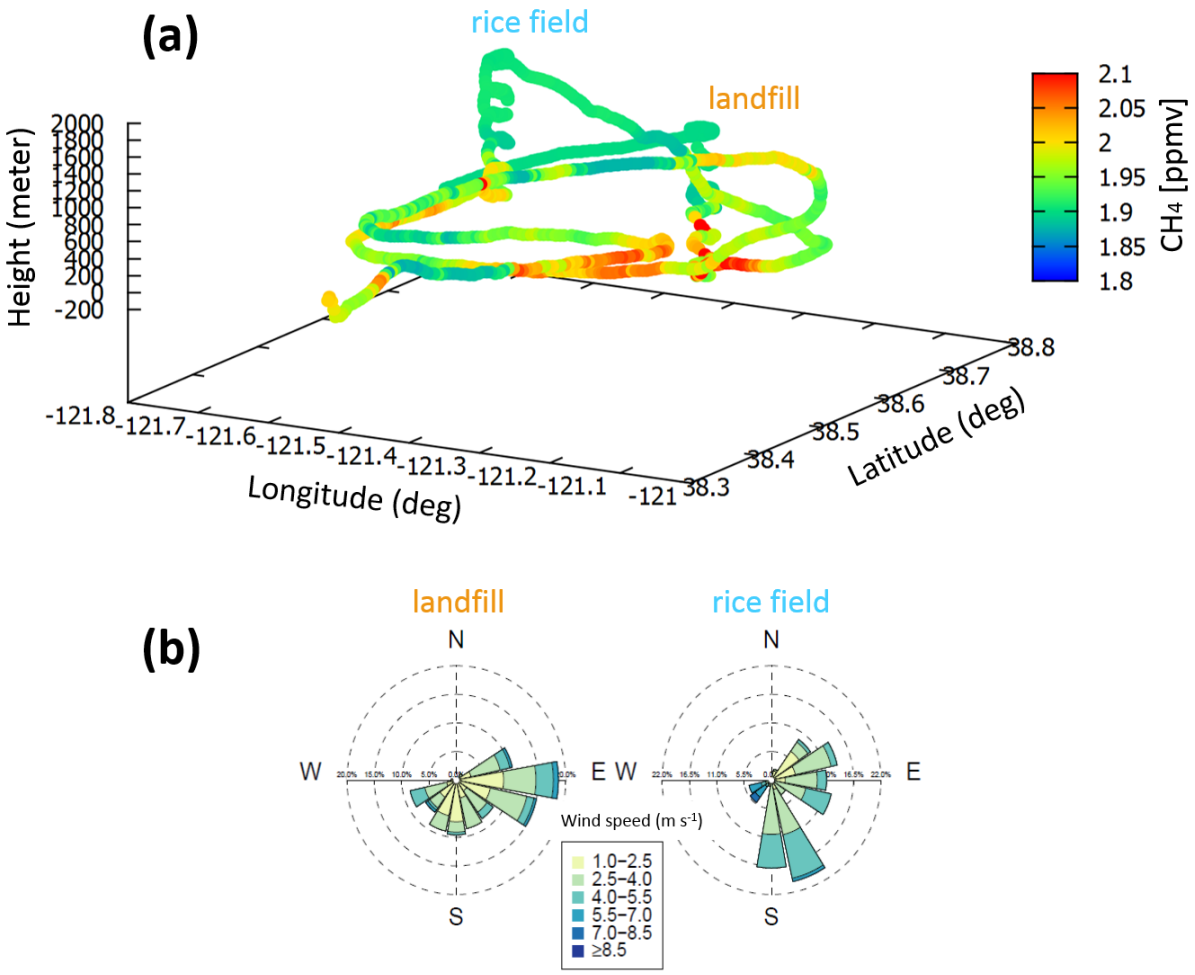

Figure S7: (a) The observed CH_4 mixing ratio over Sacramento with two local sites (landfill, rice field) and (b) Wind-rose map of the observed horizontal wind throughout the altitude over the local sitestwo local sites on July 29, 2015.

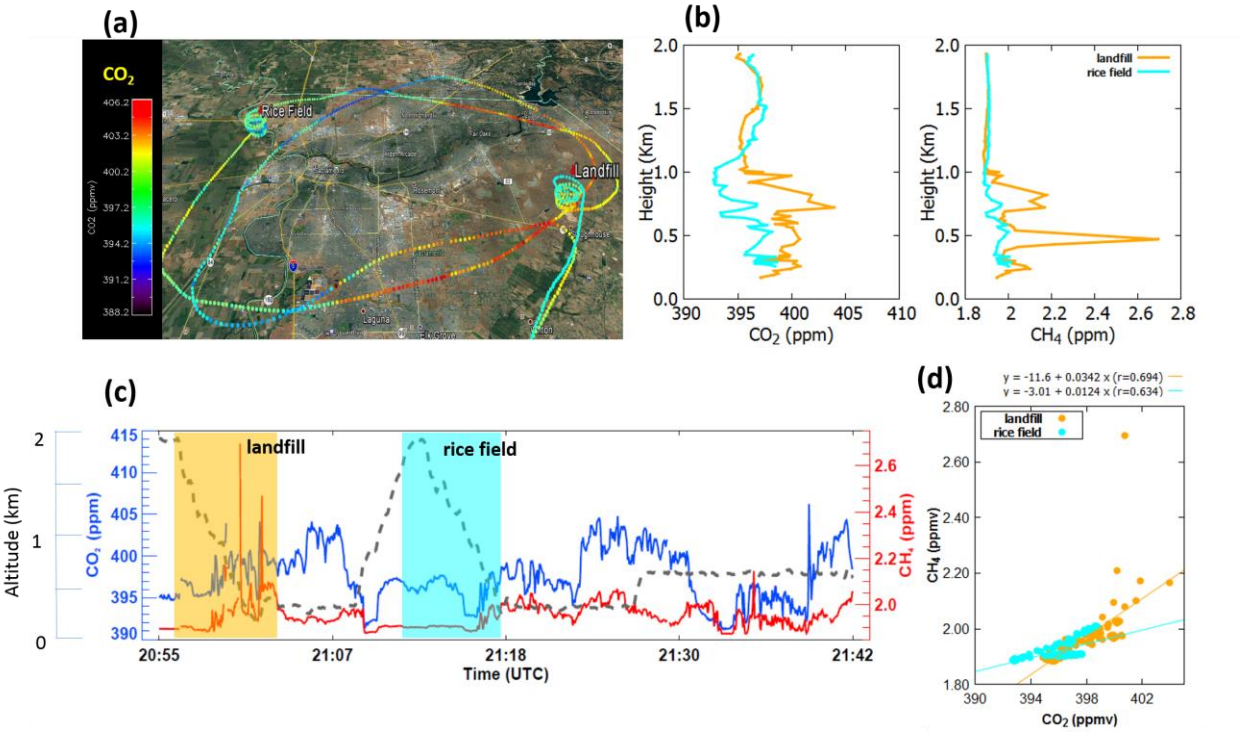

95

Figure S8: (a) Map of CO_2 mixing ratio over Sacramento with two local sites (landfill, rice field). (b) Vertical profiles of CO_2 and CH_4 mixing ratios. (c) Time series of altitude (gray), CO_2 (blue) and CH_4 (red) mixing ratio, and (d) correlation of CO_2 and CH_4 over (red) landfill, and (blue) rice field in Sacramento, CA on July 29, 2015. The shaded portions (orange and cyan) highlight the vertical profiling at two local sites.